RSC Advances

ROYAL SOCIETY OF CHEMISTRY

www.rsc.org/advances

Journal Name

RSCPublishing

ARTICLE

Exploring the effect of manganese in lead sulfide quantum dot sensitized solar cell to enhance the photovoltaic performance

Dinah Punnoose, S. Srinivasa Rao, Soo-Kyoung Kim and Hee-Je Kim*

Cite this: DOI: 10.1039/xoxxooooox

Received ooth January 2012,
Accepted ooth January 2012

DOI: 10.1039/xoxxooooox

www.rsc.org/

Herein we demonstrate for the first time, the combination of PbS with CdSe/CdS/TiO_2 and exploring the impact of manganese (Mn) on PbS (lead sulfide) quantum dot-sensitized solar cells (QDSSCs). Photo-anodes were sensitized with different percentages of Mn content (5, 10 and 15%) on PbS/CdS/CdSe using a simple successive ion layer adsorption and reaction (SILAR) technique. The performance of the QDSSCs is examined in detail using polysulfide electrolyte and a copper sulfide (CuS) counter electrode. The optimized percentage of Mn content on PbS/CdS/CdSe electrode results in higher efficiency compared to bare PbS/CdS/CdSe-sensitized QDs. This is confirmed with photovoltaic studies and electrochemical impedance spectroscopy. The 10% Mn-doped PbS/CdS/CdSe electrode exhibits short circuit current density of 17.34 mA cm^2 with an enhanced power to conversion efficiency (η) of 4.25% under 1 sun illumination (AM 1.5 G, 100 mW/cm^2).

1. Introduction

Semiconductor quantum dots (QDs) with a narrow band gap have recently attracted mounting interests in using photosensitizers as an alternative to conventional dye-sensitized solar cells (DSSCs). QDs feature tunable band gaps, a large light absorption coefficient, and high stability. [1-7] *In situ* growth methods include successive ionic layer adsorption and reaction (SILAR) [8] and chemical bath deposition (CBD)[9] ,which are the techniques often used for directly growing semiconductor QDs on mesoscopic oxide films. Inorganic semiconductor sensitizers which are typically used as QD sensitizers are currently being studied with great interest and they surpass their dye homologues. The semiconductor electrode plays an important role in collecting photo-injected electrons from the sensitizer and affords good electron transport association between the sensitizer and an external circuit.TiO_2 is a wide-band-gap semiconductor to which QDs are attached for visible light absorption.

Preceding researches show that combinations of QDs lead to higher efficiencies than pure materials. [10, 11-14] CdS, CdSe, PbS, PbSe, and Sb_2S_3 are often used as sensitizers in QDSSCs. Within these, lead sulfide (PbS) QDs have a high absorption coefficient with a tunable band gap of 0.41 eV, which could be more profitable as an effective sensitizer in QDSSCs. [15] The quantized discrete band structures, multiple exciton and theoretical efficiency which are beyond the Shockley-Queisser limit are benefits of PbS-sensitized QDSSCs. [16] On the other hand, the performance of PbS QDSSCs is much inferior than that of other semiconductor QD-based solar cells [17 -18]. These encouraging properties open windows for research in exploring and developing the performance PbS based QDSSCs. A limited passivation layer of CdS directly above the PbS-sensitized surface of the photo-anode can decrease in the recombination of photo-injected electrons with the electrolyte and boost the overall performance of the solar cells. [16] The combination of CdS/CdSe with PbS leads to better performance as a result of the re-organized step-wise band-edge levels. [19] Next, the ZnS SILAR coating technique has been used to protect QDs from photo corrosion and to suppress electron recombination with the electrolyte. By tuning their relative band alignment layer of passivized QDs this serves as main light-absorbing layer and as an electron-blocking/hole-extraction layer. [20]

In QDSSCs, several approaches are used, such as crystal size control, introducing dopants, and optimizing the QD-sensitized

electrode and the concentration of dopant, which could result in enhanced electrical and optical properties. [21-23] These properties can be enhanced by doping Mn^{2+}, Fe^{2+}, and Co^{2+} to QDs. [24] Of key importance in the exploration, the incorporation of Mn into PbS is an important methodology because it imparts paramagnetic properties. [25] Carrier-dopant exchange interactions occur in Mn doped PbS colloidal quantum dots, which leads to enhancements in both the valence and the conduction electrons. [26] Justin *et al.* worked on ZnO nano-rods with CdS/CdSe/ZnS and presented a promising passivation layer for PbS QDs which defends against polysulfide electrolyte and the large accumulation of photo-injected electrons in the conduction band of the photo-anode. This method also has low recombination of photoelectrons and in which it increases the photovoltaic efficiency [19] but there is not an appreciated enhanced efficiency.

The work of Chandu *et al.* explained the effect of manganese (Mn) doping in CdS solely without multi layered semiconductors to improve the photovoltaic performance of quantum dot sensitized solar cells and achieved 2.8% efficiency. Haining Chen *et al.* work discussed about the CdS-sensitized TiO_2 mesoporous electrode with two different sizes of CdS nanoparticles and achieved an efficiency of 1.60%.[27] However, successive layers of PbS with multi layered semiconductors (CdS/CdSe/ZnS) significantly enhances photo-currents. Comparatively, the QDSSC performance is enhanced which is attributed due to the better light harvesting ability of PbS quantum dots and makes large accumulation of photo-injected electrons in the conduction band of TiO_2. In addition to this the boosting in the photovoltaic efficiency is due to suitable amount of Mn doping to PbS.

To author's knowledge herein we report for the first time on the appropriate amount of Mn doping in PbS along with CdS, CdSe, and ZnS, which improves the photovoltaic properties of QDSSC. The morphological, optical, and structural properties of the optimized films were examined. We achieved a good photovoltaic conversion efficiency of 4.25%, which is quite high for PbS-based QDSSCs. This work paves the way for research exploring the doping effect of materials (such as manganese) in PbS with respect to TiO_2, with enhanced photovoltaic performance and stability were significantly improved. *In situ* growth methods have been widely in the preparation of PbS, CdS and CdSe QDs. The future work can be explored and investigated by employing ITO porous films as substrates for QDSSCs. [28]

2. Experimental section

2.1 Materials

Chemicals were purchased from Aldrich and used without further purification. Lead nitrate ($Pb(NO_3)_2$), manganese(II) acetate tetrahydrate [$Mn(CH_3COO)_2{\cdot}4H_2O$], cadmium acetate dehydrate [$Cd(CH_3COO)_2.2H_2O$],zincacetate dihydrate [$Zn(CH_3COO)_2.2H_2O$], sodium sulfide(Na_2S), sulfur(S), selenium (Se), copper(II) sulfate pentahydrate [$CuSO_4.5H_2O$], sodium thiosulfate ($Na_2S_2O_3$), urea (CH_4N_2O), and TiO_2 paste (Ti-Nanoxide HT/SP) were supplied by Solaronix.

2.2 Fabrication of TiO_2 photo-anodes

Fluorine-doped tin oxide glass (FTO) is used as the substrates for both the photo-anode and CE. TiO_2 photo-anodes were fabricated on ultrasonically well-cleaned FTO substrate using the doctor blade method. Anatase TiO_2 particles (Ti-Nanoxide HT/SP, Solaronix) are first deposited on the FTO substrates with an active area of 0.27 cm^2, followed by sintering at 450 °C for about 30 min. A thickness of ~7 μm is obtained. The prepared TiO_2 electrodes were used for further sensitized with PbS/CdS/CdSe/ZnS and Mn-d-PbS-CdS-CdSe-ZnS.

2.3 Fabrication of PbS/CdS/CdSe/ZnS and Mn-d-PbS/CdS/CdSe/ZnS sensitized photo-anodes

The PbS and CdS/CdSe QDs were sensitized on TiO_2 using the SILAR technique.[8] The TiO_2 photo-anodes were immersed in a solution containing 25 mM $Pb(NO_3)_2$ for 5 minutes to allow Pb^{2+} ions to adsorb, and then it is rinsed with DI water and ethanol to remove the excess Pb^{2+} ions. Photo-anodes were then dipped into an aqueous solution containing 0.1 M sodium sulfide (Na_2S) for 5 minutes, where the pre-adsorbed Pb^{2+} ions react with S^{2-} ions to form PbS. Then, the electrodes were rinsed with DI water and ethanol and dried under N_2 gas. These two dipping procedures constitute one cycle, and two cycles were applied. More number of PbS cycles decreased the efficiency. Hence we fixed two successive layers. Fig. 1 shows a schematic diagram of the SILAR processes. For the doping of Mn^{2+}, proper molar percentages of (5, 10 and 15%) Mn $(CH_3COO)_2{\cdot}4H2O$ were mixed with the $Pb(NO_3)_2$ to enable the co-adsorption of Mn^{2+} and Pb^{2+} ions. Then, CdS is sensitized for five cycles using an aqueous solution of 0.1 M cadmium acetate dihydrate and 0.1 M Na_2S to achieve good adsorption over the PbS/TiO_2 photo-anode. For the deposition of CdSe QDs, the $CdS/PbS/TiO_2$-sensitized photo-anode is immersed in an aqueous solution of 0.1 M cadmium acetate dihydrate and 0.2 M Na_2SeSO_3

for about 8 cycles. Then, the QD-deposited photo-anodes were washed with DI water and dried in N_2 gas. Finally, two cycles of ZnS passivizing layers were coated over the CdSe/CdS/PbS and CdSe/CdS/ Mn-d-PbS sensitized photo-anodes by the SILAR method using an aqueous solution of 0.1 M Zn $(NO_3)_2$ and 0.1 M (Na_2S), and each is dipped for 5 min per cycle and washed several times, dried, and used for the fabrication of QDSSCs. The ZnS can proficiently cover the bare TiO_2 and QDs, resulting in strong inhibition of the electron leakage from either the QDs or TiO_2 to the electrolyte.

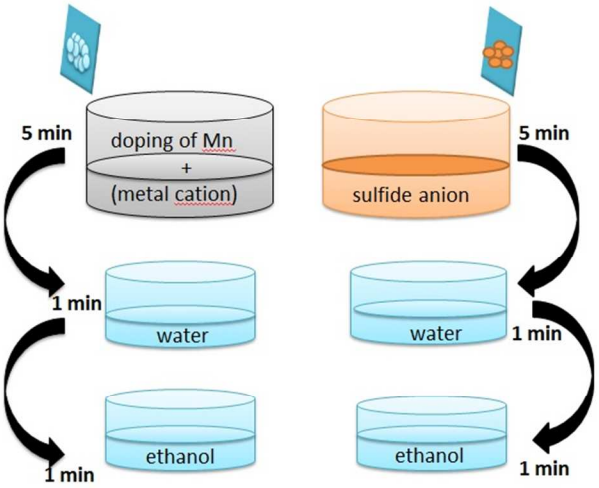

Fig. 1 SILAR processes

2.4 Fabrication of a counter electrode

CBD is a modest and easy method for preparing the metal sulfide CE and FTO substrate. [9] Prior to deposition, the FTO samples were cleaned ultrasonically using acetone, ethanol, and DI water for 10 minutes each. The prepared substrates were dried with N_2 gas. A CuS aqueous solution is prepared using 0.1 M $CuSO_4.5H_2O$ and 0.4 M $Na_2S_2O_3$ as sources of Cu^{2+} and S^{2-} ions. 0.4 M CH_4N_2O is used as a reagent for depositing CuS thin films. The substrates were then dipped horizontally into the solutions of CuS and kept in a hot air oven at 65 °C for about 2 h. The CuS-coated films were washed several times with DI water and ethanol.

2.5 Assembly of PbS/CdS/CdSe/ZnS , Mn-d-PbS/CdS/CdSe/ZnS QDSSC

The PbS-CdS-CdSe-ZnS, Mn-d-PbS/CdS/CdSe/ZnS QD-sensitized TiO_2 electrode and the CuS CE were assembled and sealed in layers using a transparent 50-µm hot melt sealing sheet (double sheet of SX 1170-25, Solaronix). Polysulfide electrolyte is injected through a pin-hole made in the CE. The cells were left for a few hours to complete the diffusion of electrolyte within the photo-anode, and the cells were tested under one sun illumination (AM 1.5 G, 100 mW/cm^2)

2.6 Characterizations

The surface morphology of the thin films were characterized using a field emission scanning electron microscope (FE-SEM, S-4200, Hitachi) equipped with energy dispersive X-ray spectroscopy (EDS) at an operating voltage of 15 kV to determine the elemental composition. QD adsorption is measured by UV-Vis spectroscopy (Mecasys, OPTIZEN 3220UV) over the wavelength range of 300-800 nm. The current-voltage characteristics of the QDSSCs were investigated under 1 sun illumination (AM 1.5G, 100 mW cm^{-2}) using an ABET Technologies (USA) solar simulator. Electrochemical impedance spectroscopy (EIS) is also used on the QDSSCs with CuS CEs using a BioLogic potentiostat/ galvanostat/EIS analyzer (SP-150, France) under 1 sun illumination. The frequency ranged from 100 mHz to 500 kHz. XPS analysis was performed using an X-ray photoelectron spectrometer (VG, ESCALAB 250) with monochromatic Al Ka radiation (hn = 1486.6 eV)

3. Results and discussions

The general structure of the QDSSC is shown with details in Fig. 2. The cells are composed of the QD sensitized electrodes, the polysulfide electrolyte and CuS counter electrode and its details of the core shell QDSSCs.Due to the easy corrosion of the metal chalcogenides in the idodide/triodide electrolyte, polysulfide is the best choice for QDSSCs. Upon 1 sun illumination (100 mW cm^{-2}), photons are captured by the QDs, which generates excitons, drives electrons toward the TiO_2 conduction band, and transfers holes to electrolyte. The injected electrons travel through the semiconductor and the back contact, and then through the load to the CE.

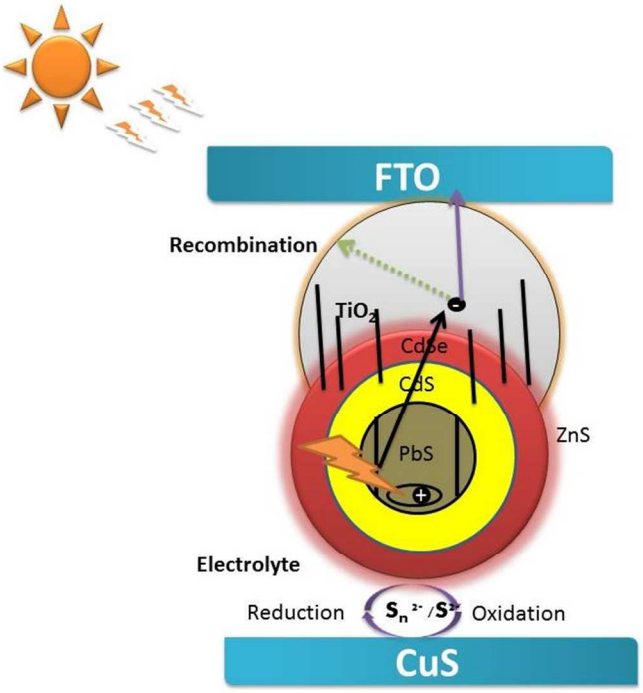

Fig.2. (a) Graphical representation of Mn-d-PbS/CdS/CdSe/ZnS on QDSSC with CuS counter electrode and polysulfide electrolyte and its details

3.1. Structural and morphological studies

Scanning electron microscopy (SEM) revealed the surface morphology of the bare PbS/CdS/CdSe/ZnS and the 5, 10, 15 molar % Mn-d-PbS/CdS/CdSe/ZnS on TiO_2, as shown in Fig.3.The bare PbS/CdS/CdSe/ZnS electrode has a uniformly distributed scale-like nanostructure and thus a high surface area on the TiO_2 surface (Fig. 3a). When 5% Mn is doped into PbS-CdS-CdSe-ZnS, the surface structures become closer than with the PbS/CdS/CdSe/ZnS QDs (Fig. 3b). The gaps between the scale-like nanostructures were reduced by increasing the Mn concentration percentage, which decreased the recombination, leading to increased efficiency.

The 10% Mn-d-PbS/CdS/CdSe/ZnS features with a large number of scale-like nanostructures (Fig. 3c), which could improve the photovoltaic performance. When the deposition molar percentage of Mn is increased to 15% (15% Mn-d-PbS-CdS-CdSe-ZnS), the gaps between the scale-like nanostructures again started to form (Fig. 3d). The amount of adhesion of the active materials on FTO is a vital factor in determining the efficiency of the QDSSCs. If the materials do not stick to the FTO, they may peel off from the FTO substrate and release into the electrolyte, thus decreasing the efficiency of the QDSSCs. [29] The efficiency of the QDSSCs is improved by changing the surface morphology of the electrode from compact to porous, as well as by the particle-ornamented surface architecture.

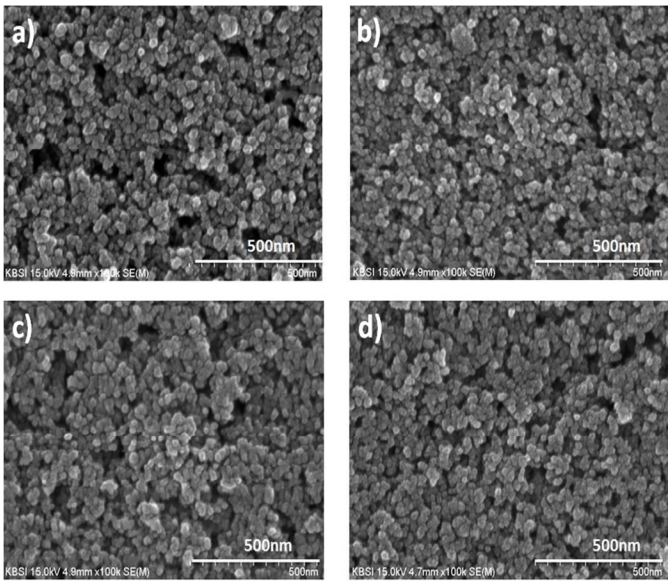

Fig. 3. SEM images of (a) PbS-CdS-CdSe-ZnS, (b) 5% Mn-d-PbS-CdS-CdSe-ZnS, (c) 10% Mn-d-PbS/CdS/CdSe/ZnS (d) 15% Mn-d-PbS/CdS/CdSe/ZnS sensitized electrodes on the surface of TiO_2.

To examine the crystal structure and phase purity of the thin films, they were examined using XRD analysis. The XRD results of the bare PbS/CdS/CdSe/ZnS and 5, 10, and 15% Mn-d-PbS/CdS/CdSe/ZnS films on TiO_2 are shown in Fig.4.

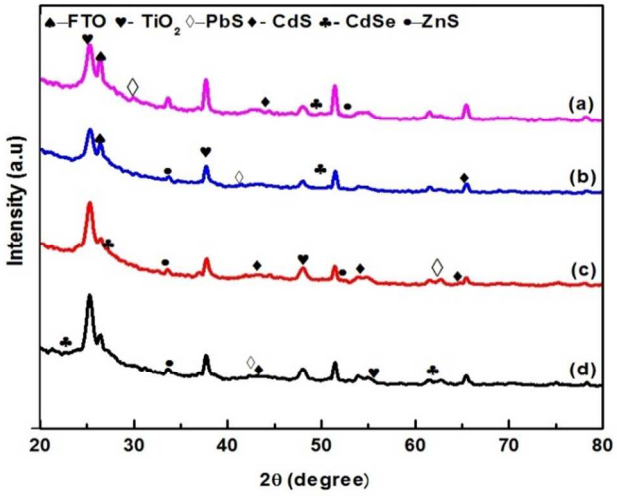

Fig. 4 XRD pattern of (a) PbS/CdS/CdSe/ZnS (b) 5% Mn-d-PbS-CdS-CdSe-ZnS, (c) 10 % Mn-d-PbS/CdS/CdSe/ZnS and (d) 15% Mn-d-PbS/CdS/CdSe/ZnS sensitized electrodes on the surface of TiO_2

The sensitized films were dried in air and examined without calcination. The detailed observations and corresponding planes are shown in Table1. All of the diffraction peaks match well with the standard XRD pattern obtained through the preparation process. The spade symbols in the figure represent the FTO glass substrate peaks. However, the XRD pattern of the films did not exhibit any characteristic peaks, which might be due to the very low thickness of the materials or interference from the XRD signals of the high crystallinity FTO substrate. [30] Moreover, the presence of Mn is confirmed from the XPS analysis, which is shown in Fig. S1.†

Table 1 Shows the detailed XRD analysis of PbS/CdS/CdSe/ZnS thin film

S.NO	Name	2θ(degrees)	JCPDS card no and its corresponding planes
1	TiO_2	25.272, 37.799, 48.049, 53.331	001-084-1286 [1 0 1] [0 0 4] [2 0 0] [1 0 5]
2	PbS	30.072, 43.053, 62,525	05-0592 [2 0 0] [2 2 0] [4 0 0]
3	CdS	44.0320, 54.622, 64,003	01-080-0019 [2 2 0] [2 2 2] [4 0 0]
4	CdSe	23.788, 27,679, 52,144, 63,786	01-077-2309 [1 0 0] [1 0 1] [0 0 4] [2 0 3]
5	ZnS	33.65, 35.567, 52.003	00-039-1363 [1 0 5] [1 0 6] [1 0 12]

EDX analysis was conducted to investigate the elemental compositions of PbS/CdS,CdSe/ZnS and Mn-d-PbS/CdS/CdSe/ZnS QD sensitizers on TiO_2, and the results are shown in Fig. 5. The elements in the TiO_2 were also detected due to the lower deposition of PbS/CdS,CdSe/ZnS QDs. The analysis shows the purity of the sample. There is no impurity detected in the sample, since there are no elements except for Pb, Cd, Se, Zn S, and Mn in the EDX spectrum. The Pb, Cd, Se, Zn S, and Mn orbital states are seen in the EDX spectrum. The film in Fig.5(a) contains atomic percentages of Pb and 13% S, indicating an atomic ratio of approximately 1:1 for Pb vs. S. Fig. 5(b) shows that upon ion exchange, 0.9% Mn content emerges in the film, while the Pb content drops from 15% to 14%, indicating the occurrence of ion exchange from Pb to Mn. The amount of dopants present in the Mn-d-PbS/CdS/CdSe/ZnS reveals that the Mn concentration increases with the increase in dopant. In figures 5(b), (c), and (d), the energy levels of Mn at 6.23 KeV, and 6.536 217 KeV correspond to Kα, and Kαβ, respectively.

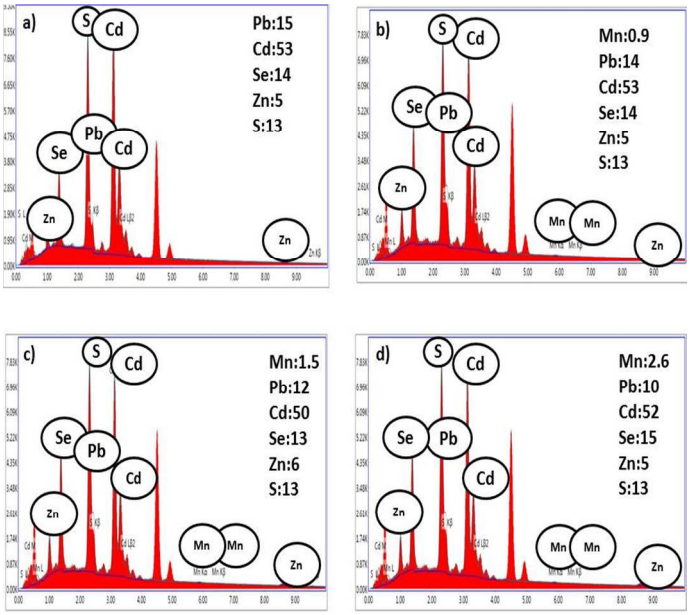

Fig. 5 Energy dispersive X-ray spectroscopy of (a) PbS/CdS/CdSe/ ZnS(b) 5% Mn-d-PbS-CdS-CdSe-ZnS, (c) 10 Mn-d-PbS/CdS/CdSe /ZnS and (d) 15% Mn-d-PbS/CdS/CdSe/ZnS sensitized electrodes

3.2. Optical properties

The UV-Vis absorption spectra of the PbS/CdS/CdSe/ZnS and Mn-d-PbS/CdS/CdSe/ZnS QD-sensitized electrodes are shown in Fig. 6. The absorption edge of the TiO_2 photo-anode appears at about 360 nm. The absorption of the bare PbS/CdS/CdSe/ZnS photo-anode is near 600 nm, and those of the 5%, 10%, and 15% Mn-d-PbS/CdS/CdSe/ZnS are a little shifted towards longer wavelengths. The intensity of the absorbance is higher for the 10% Mn-d PbS/CdS/ CdSe /ZnS than for the bare PbS/CdS/CdSe/ZnS photo-

anode and 5% and 15% Mn-d-PbS-CdS-CdSe-ZnS. This indicates that the addition of manganese to the PbS/CdS/CdSe/ZnS QDs can improve the light harvesting ability of the photo-anode. This improvement could be due to the slightly broader size distribution in the doped sample or the incorporation of Mn ions into the crystal lattice of PbS.

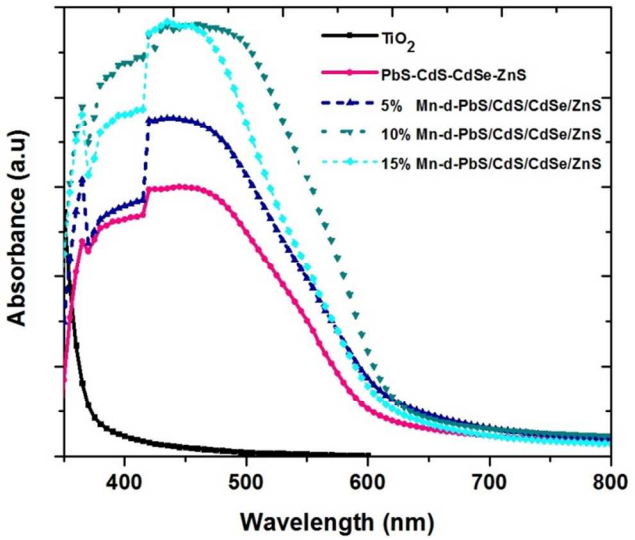

Fig.6 UV- vis absorption spectra of (a) PbS/CdS/CdSe/ZnS (b) 5% Mn-d-PbS-CdS-CdSe-ZnS, (c) 10 Mn-d-PbS/CdS/CdSe/ZnS (d) 15% Mn-d-PbS/CdS/CdSe/ZnS sensitized electrodes on the surface of TiO_2

The higher percentage of Mn doping could not increase the absorption. An increase in Mn-content induces a systematic increase of and a monotonic decrease of the degree of circular polarization (DCP) of the QD photo luminescence emission.[31] The device stability is found to depend more on the interface and band alignment between the QDs and anodes rather than on the bulk QD layer itself.[20] The band gap of PbS (1.55 eV), CdS (2.52 eV) and CdSe (2.17 eV) is obtained from the absorption spectrum and it is higher than that of bulk by the indication of the quantum confinement effect. To better understand the flow of excited electrons the energy band gap alignment diagram for the combined QDs is shown in Fig. S2.†

3.3 Performance of QDSSC

3.3.1. Photovoltaic analysis

The deposition and optimization of the PbS/CdS/CdSe/ZnS and the 5, 10, 15% Mn-d-PbS/CdS/CdSe/ZnS on the TiO_2 surface were conducted. The cells were fabricated using FTO/TiO_2/PbS-CdS-CdSe-ZnS, Mn-d-PbS/CdS/CdSe/ZnS and a polysulfide electrolyte as the hole transporter. The current density-voltage (J-V) curves were obtained under one-sun illumination. The photocurrent of the electrodes changes a little as the molar percentage of Mn is increased, indicating that the high amount of Mn incorporation affects the absorbance of visible light and induces a higher current density. This also shows that an optimal amount of Mn must be doped in the PbS-CdS-CdSe-ZnS.The short-circuit current density (J_{SC}) increases continuously with the molar percentage of Mn in PbS/CdS/CdSe/ZnS up to 10%. Additional deposition of Mn decreases the overall power conversion efficiency, since the augmented pore filling affects the electrolyte dissemination within the TiO_2 film. The J-V curves of optimized PbS/CdS/CdSe/ZnS and Mn-d-PbS/CdS/CdSe/ZnS cells under one full sun (100 mW/cm^2) are shown in Fig. 7. Photovoltaic parameters like V_{OC}, J_{SC}, fill factor (FF), and total energy conversion efficiency (η) are listed in Table 2.

Table 2 Summary of the photovoltaic properties of Mn-d-PbS/CdS/CdSe/ZnS and undoped PbS/CdS/CdSe/ZnS electrodes with CuS counter electrode

Parameter	PbS/CdS/CdSe/ZnS	5% Mn-d-PbS/CdS/CdSe/ZnS	10%Mn-d-PbS/CdS/CdSe/ZnS	15%Mn-d-PbS/CdS/CdSe/ZnS
V_{OC}	0.51	0.52	0.53	0.51
J_{SC}(mA cm-^{2})	15.3	16.11	17.34	16.76
FF	0.475	0.474	0.48	0.481
η(%)	3.86	4.06	4.25	4.14

The QDSSC with a bare photo-anode demonstrates a V_{OC} (0.51 V), J_{SC} (15.3 mA/cm^2), FF (0.48) and η (3.86%). V_{OC} and FF of the QDSSCs with 5% Mn-d-PbS-CdS-CdSe-ZnS, 10% Mn-d-PbS-CdS-CdSe-ZnS, and 15% Mn-d-PbS/CdS/CdSe/ZnS photo-anodes are slightly higher than those with the CdS photo-anode, resulting in higher η values of 4.06%, 4.25%, and 4.14%, respectively. The main reason for enhanced photovoltaic properties is that the Mn impurities have a drastic impact on the host material and can create new energy states that can delay the exciton recombination time and can allow charge separation. V_{OC} can be

calculated using the potential difference between the Fermi energy levels near the conduction band edge and the redox potential of the electrolyte. Consequently, the pre-treated interfacial doped buffer layers can help the electron accumulation inside the TiO_2 photo-anode. [24]

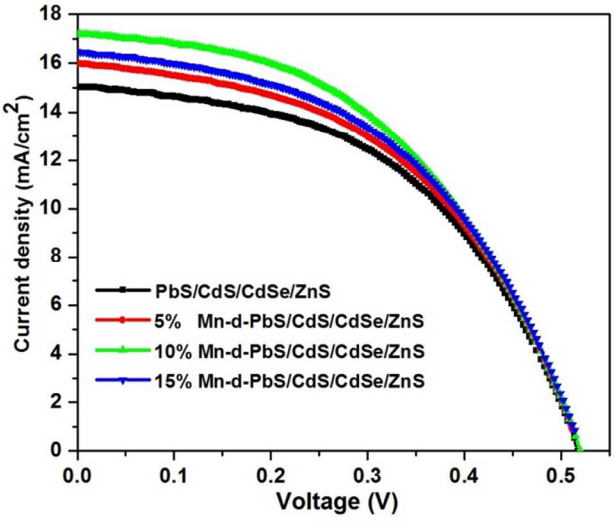

Fig.7 The photocurrent density-voltage curves of bare PbS/CdS/CdSe/ZnS and 5, 10, 15% Mn-d- PbS/CdS/CdSe/ZnS photoanode with CuS counter electrode.

The produced photo electrons are expected to transfer to the electrolyte and combine with $S_n^{2-}$to form nS^{2-} to promote redox reactions in the electrolyte which is shown in Fig. 8.It is important how effectively the QDS can accept the light .The photo physical properties can be improved easily by the impurities.

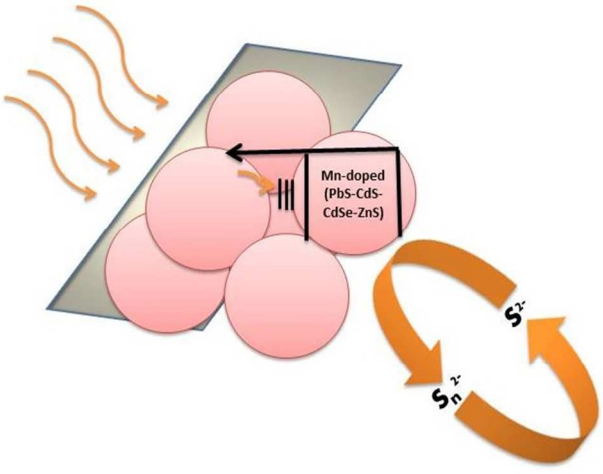

Fig. 8 Mechanism for the supply of photo electrons from the Mn-d-PbS/CdS/CdSe/ZnS electrode.

Fig.9 shows the IPCE spectra of QDSSCs based on bare PbS/CdS/CdSe/ZnS and 5, 10, 15% Mn-doped PbS/CdS/CdSe/ZnS electrodes. the highest IPCE value is 95% at ~500 nm for 10% Mn-doped PbS/CdS/CdSe/ZnS QDSSC which is higher than that of bare PbS/CdS/CdSe/ZnS and 5,15%Mn-doped PbS/CdS/CdSe/ZnS based QDSSCs. The large IPCE value of 10% Mn-doped PbS/CdS/CdSe/ZnS QDSSC is ascribed due to the enhancement of light-harvesting efficiency by the Mn doped PbS QDs. This results in more electron collection, easy transfer of electron to the conduction band of TiO_2 and less recombination of photo excited electrons with the electrolyte. [32]

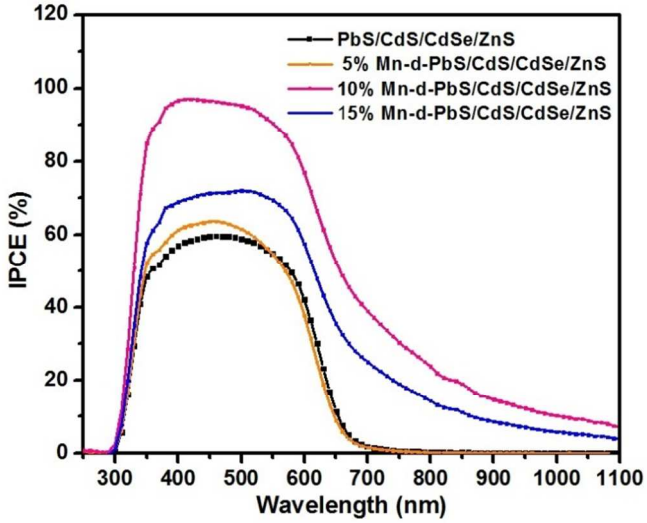

Fig. 9 IPCE spectrum of bare PbS/CdS/CdSe/ZnS and 5, 10, 15% Mn-d- PbS/CdS/CdSe/ZnS photoanode sensitised TiO_2 QDSSCs.

3.3.2. Electrochemical impedance studies

Electrochemical impedance spectroscopy (EIS) is a powerful tool for characterizing the performance of each component of QDSSCs, and it is used to investigate the interior resistance and charge transfer kinetics of QDSSCs. The Nyquist plots of QDSSCs with PbS/CdS/CdSe/ZnS and Mn-doped PbS/CdS/CdSe/ZnS photo-anodes were measured under a simulated light source. The plots were analyzed using Z-view software with an equivalent circuit as shown in Fig. 10.

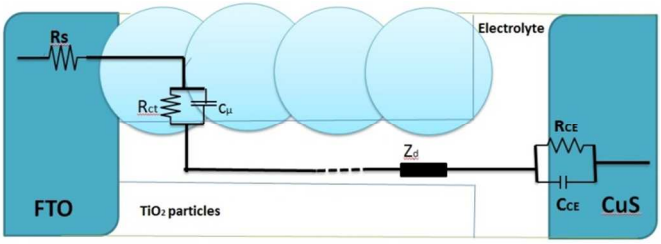

Fig. 10 Equivalent circuit diagram of QDSSC

The equivalent circuit diagram model consists of, the series resistance (R_S) is the non-zero intercept on the real axis of the plot. It represents the sheet resistance of the transparent conducting film (TCO) and the resistance of the FTO/TiO_2. The electron transfer resistance (R_{ct}) is at the photo-anode/electrolyte interface, and it is parallel with the chemical capacitance (Cμ). The finite Warburg impedance (Z_d) elements are associated with diffusion processes, which are influenced by the behaviour of the porous electrode/electrolyte interface and the counter electrode/electrolyte. Z_d in the lowest frequency region is because of the Warburg impedance of the redox couple in the electrolyte. [33] The R_{CE} and C_{CE} are related to counter electrode resistance and capacitance.

To understand the carrier transport dynamics in these devices the EIS parameters are determined. The parameters obtained from the EIS analysis are shown in Table 3. The 10% Mn-d-PbS/CdS/CdSe/ZnS photo-anode has the highest charge transfer resistance R_{ct} (50.01 Ω) among the other electrodes and the highest chemical capacitance Cμ (3977 μF), shown in Fig.11 indicating more rapid charge transport at the TiO_2/electrolyte/QD interface. This is mainly related to the large collection of photo exited electrons into the conduction band of photo-anode, which is responsible for large current density of the cell. [34]

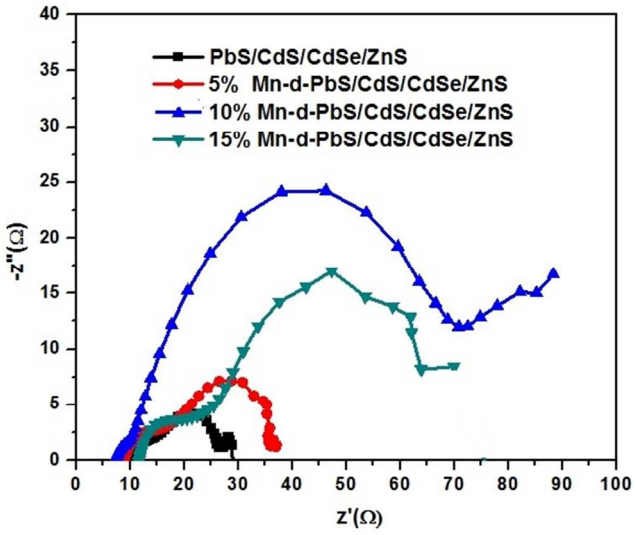

Fig. 11 EIS spectra of QDSSCs based on bare PbS/CdS/CdSe/ZnS and 5, 10, 15% Mn-doped PbS/CdS/CdSe/ZnS electrodes measured at the frequency range 100 mHz–500 kHz.

The bare PbS/CdS/CdSe/ZnS has lower R_{ct} (11.17 Ω) and the lowest Cμ (1402μF) because of the much lower electron transfer at the TiO_2/QDs/electrolyte interface.[35] This revels that hetero structured photo-anode conquers the recombination of photo injected electrons with the redox electrolyte and making large number of electrons accumulated in the photo-anode resulting to prevent the declanation of V_{OC} of Mn doped PbS based cell.[36,37] The increasing R_{ct} with the increase in Mn ions leads to higher resistance (50.1 Ω) of the photo-anode. The reduced Cμ indicates lower electron density due to the absence of Mn ions.[24] The higher Z_d is because the thicker porous Mn-d-PbS/CdS/CdSe/ZnS materials increased the diffusion length.

Table 3 Summary of the photovoltaic properties and EIS results of Mn-d- PbS/CdS/CdSe/ZnS and undoped PbS/CdS/CdSe/ZnS electrodes with CuS counter electrode.

Parameter	PbS/CdS/CdSe/ZnS	5%Mn-d-PbS/CdS/CdSe/ZnS	10%Mn-d-PbS/CdS/CdSe/ZnS	15%Mn-d-PbS/CdS/CdSe/ZnS
Rs (Ω)	9.6	9.58	7.24	8.36
R_{CE}(Ω)	4.9	7.45	4.04	22.42
Rct(Ω)	11.17	16.9	50.01	34.01
Cμ(μF)	1402	3901	3977	3899
Zw(Ω)	1.8	2.3	20.18	7.63

The Bode phase plots for cells with different configurations are shown in Fig. 12. The electron life times (τ_r) can be obtained according to the following equation:

$$\tau_r = 1/(2\pi f_{max}), \quad (1)$$

where f_{max} is the maximum frequency of the middle-frequency peak in the Bode plot. The τ_r values of bare PbS/CdS/CdSe/ZnS and 5, 10, 15% Mn-doped PbS/CdS/CdSe/ZnS were found to be 25.36, 31.74, 49.8 and 46.2 ms, respectively. The higher τ_r value of the 10% Mn-doped PbS/CdS/CdSe/ZnS suggests that electrons have a longer lifetime and are effectively transferred, resulting in higher J_{SC} and energy conversion efficiency for the QDSSC. The frequency peak of 10% Mn-doped PbS/CdS/CdSe/ZnS shifted to lower frequency, which is ascribed to the enhanced electron transport. Electrons with higher mobility can travel a longer distance with fewer surface traps.

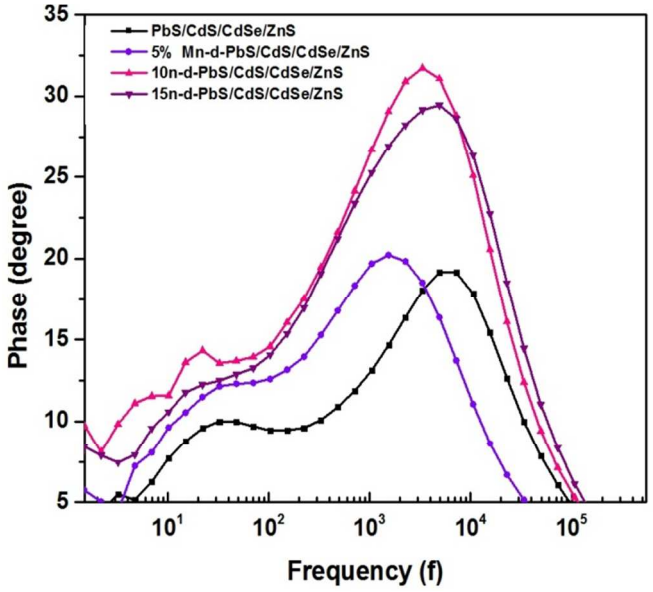

Fig. 12 Bode plot of QDSSCs based on bare PbS/CdS/CdSe/ZnS and 5, 10, 15% Mn-doped PbS/CdS/CdSe/ZnS electrodes measured at the frequency range 100 mHz–500 kHz.

EIS spectra of QDSSCs based on bare PbS/CdS/CdSe/ZnS and 5, 10, 15% Mn-d-PbS/CdS/CdSe/ZnS electrodes at the applied forward bias potential of 0.7 V under dark condition is shown in Fig. 13.The two semicircles can be recognized and fitted according to an equivalent circuit model. It can be seen that the R_{CE} values are similar, for both Mn-doped and undoped PbS/CdS/CdSe/ZnS QDs sensitized photo-anodes.From the plot it is seen that the diameter of the lower frequency semicircle decreases with applied bias voltage. At bias condition, the electrons are injected into conduction band of the TiO_2 photo-anode and recombine with the redox electrolyte. Therefore, the decrease of lower frequency semicircle under applied bias can be explained as the change of the number of electrons recombining with the electrolyte at the TiO_2/electrolyte interface. The 10% Mn-d-PbS/CdS/CdSe/ZnS photo-anode QDSSC shows that the lower frequency arc is less than that of PbS/CdS/CdSe/ZnS and 5, 15% Mn-d-PbS/CdS/CdSe/ZnS

The R_{ct} (47 Ω) value of the 10% Mn-d-PbS/CdS/CdSe/ZnS QDSSC is higher than that of the PbS/CdS/CdSe/ZnS (18 Ω), so the dark reaction in the QDSSC sensitized with Mn-d-PbS/CdS/CdSe/ZnS QDs can be suppressed more efficiently than that of the sample sensitized with pure PbS/CdS/CdSe/ZnS QDs. One more reason may be due to large recombination of electrons with the electrolyte. This tends to reduce large injection and accumulation of photo exited electron in the conduction band of the photo-anode. Therefore, electron recombination would be much more serious at the photo-anode/electrolyte interface for the QDSSC based on PbS/CdS/CdSe/ZnS than those for the QDSSCs based on 5, 10 and 15% Mn-doped PbS/CdS/CdSe/ZnS electrodes and shorter electron lifetime should be expected.[38] The relatively high values of R_{ct} yields the excellent value of lifetime of 10% Mn-d-PbS/CdS/CdSe/ZnS which contributes to keep V_{oc} at a high level by avoiding electron loss in the semiconductor.[39] The appropriate quantity of Mn leads to an increased electron transfer process and improved efficiency of the solar cells.

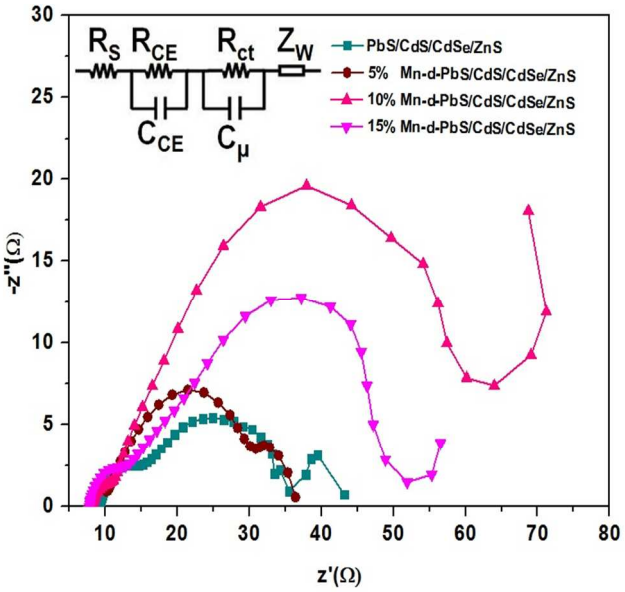

Fig.13 EIS spectra of QDSSCs based on bare PbS/CdS/CdSe/ZnS and 5, 10, 15% Mn-doped PbS/CdS/CdSe/ZnS electrodes measured at the frequency range 100 mHz–500 kHz at the applied forward bias potential of 0.7 V under dark condition.

3.4 Stability

The device stability is often ignored, but it is very important for any real world applications. The stability is checked for the PbS/CdS/CdSe/ZnS and 10% Mn-d- PbS/CdS/CdSe/ZnS photo-anodes with the CuS CE. Fig. 14 shows a comparison of the photovoltaic parameters (V_{OC}, J_{SC}, FF, and η) of the PbS/CdS/CdSe/ZnS and 10% Mn-d-PbS/CdS/CdSe/ZnS curves extracted from 24 h stability tests. The solar cell devices were stored in air with light illumination and without wrapping. The η values of the PbS/CdS/CdSe/ZnS photo-anode declined continuously within 24 h, whereas the power conversion efficiency values of the 10% Mn-d-PbS/CdS/CdSe/ZnS photo-anode increased in the first 2 h from 4.2% to 4.4% and decreased from 4.3% to 4.06% for another 8 h. However, excellent constant η values were maintained after that. The performance increases during the first two hours of air exposure after evaporation of the electrodes. The origin of this initial increase

is still under investigation. The mid-gap states created by Mn doping cause electrons to become trapped, and they are screened form charge recombination with holes and the oxidized polysulfide electrolyte.

The enhanced photo-stability of Mn-d-PbS/CdS/CdSe/ZnS could be attributed to the hole-scavenging capability of the polysulfide electrolyte, which suppresses hole-induced anodic corrosion. Efficient photoelectron supply from the CE reduces the rate of recombination and causes electron accumulation in the conduction band of TiO_2, thereby increasing Voc and Jsc. As a result, a PCE of 4.25% is obtained with the Mn-d-PbS-CdS-CdSe-ZnS, which is higher than that of the bare PbS/CdS/CdSe/ZnS (3.86%). This result indicates that the performance of the QDSSC is improved by doping with an appropriate amount of Mn in the photo-anode electrode material.

The PCE improvement is likely derived from two factors: reduced recombination losses due to the combination of Mn and PbS passivation. A more complete passivation of QD surfaces is also a likely reason for the improved device stability.

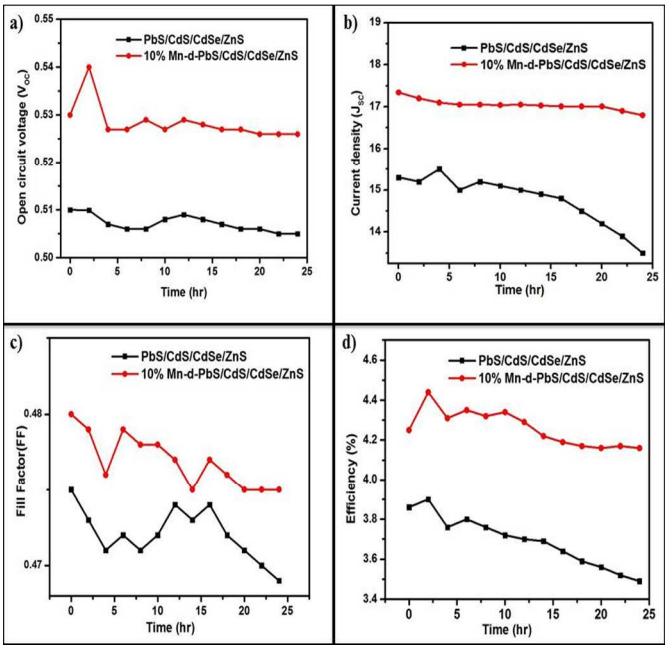

Fig.14 Stability test: Evolution of photovoltaic parameters values, (a) Voc, (b) Jsc, (c) FF, and (d) η for the QDSSC based on PbS/CdS/CdSe/ZnS, Mn-d- PbS/CdS/CdSe/ZnS electrodes**.**

We have demonstrated high-performance QDSSC through engineering of the band alignment at the QDs and the QDs/anode interface. These solar cells were processed in air at room temperature and exhibit excellent stability. We expect that determining the origin of the low V_{OC} and optimizing the combinations of Mn with PbS and QDs will result in continued efficiency improvements. Greater understanding of the QD optoelectronic properties and further progress in materials with the optimisation of counter electrodes [40-44] could lead to the generation of much more stable QDSSCs with higher efficiency.

Conclusion

We have fabricated Mn-doped PbS/CdS/CdSe/ZnS QDs on the surface of TiO_2 by the facile SILAR method. We obtained a detailed comparison between PbS/CdS/CdSe/ZnS and Mn-d-PbS/CdS/CdSe/ZnS photo-anodes, which revealed that Mn-d-PbS/CdS/CdSe/ZnS can achieve large accumulation of photo-injected electrons in the conduction band of the photo-anode with low recombination of photo-generated electrons. This is enabled by faster charge transport, more efficient charge separation, lower recombination resistance, and greater stability. A short circuit density of 17.34 mA cm^{-2} and conversion efficiency of 4.25% under one sun illumination were achieved by the QDSSC with 10% Mn doping in PbS-CdS-CdSe-ZnS. This doping level enabled improvement in the power conversion efficiency compared to undoped films (bare PbS-CdS-CdSe-ZnS). This result confirms that this amount of Mn ions on the PbS/CdS/CdSe/ZnS is very effective for improving both the chemical stability and electronic surface state by reinforcing the surface area in the QDSSCs.

Acknowledgements

This research is supported by Basic Science Research Program through the National Research Foundation of Korea (NRF) funded by the Ministry of Education, Science and Technology (2011-0014437).

Notes and references

Department of Electrical and Computer Engineering, Pusan National University, Gumjeong-Gu, Jangjeong-Dong, Busan 609-735, South Korea

† Footnotes should appear here. These might include comments relevant to but not central to the matter under discussion, limited experimental and spectral data, and crystallographic data.

Electronic Supplementary Information (ESI) available: [From XPS analysis (Fig.S1) the successful doping of Mn over PbS/CdS/CdSe/ZnS can be confirmed. XPS was measured to know the composition and chemical bond configuration of elements present in Mn-d-PbS/CdS/CdSe/ZnS. Fig. S1(i) and

S1(ii) shows the binding energy peaks at 653.9eV for Mn $2p_{1/2}$ and 137.8 eV for Pb $4f_{7/2}$ which is well in agreement with the previous reports. [1,2] The XPS clearly detects and confirms the presence of Mn, whereas the Mn peak is not detected in the XRD pattern.

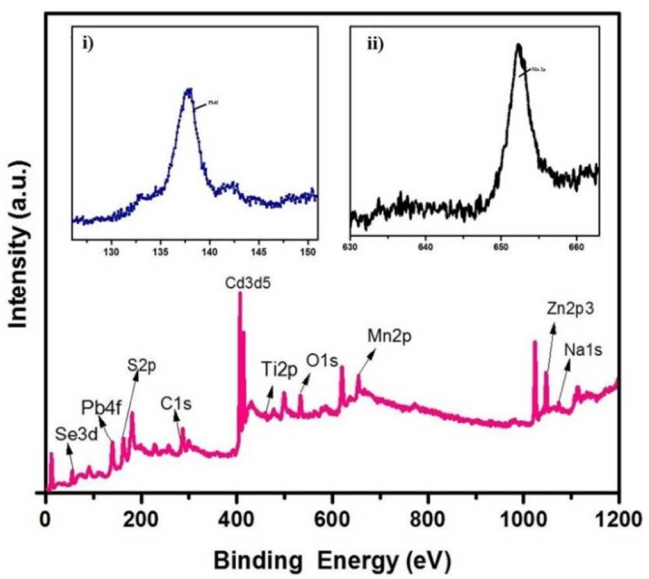

Fig.S1 XPS survey of 10 % Mn-doped PbS/CdS/CdSe/ZnS films; inset shows the (i) Mn and (ii) Pb binding energy peaks.

From the band gap, the possible electron transfer mechanism in the photo-anode is expected using the previous reports [3, 4] and schematically depicted in Fig. S2. In Mn doped PbS sensitized solar cells, the low band gap of bulk PbS shows an inability of electron transfer to the conduction band of the semiconductor photo-anode i.e., the conduction band position of PbS is much lower than that of semiconductor. But in case of PbS quantum confinement the conduction band of PbS tend to an upshift, allowing the fast electron into the semiconductor photo-anode. [5-7] Furthermore, the band position of bulk PbS, CdS and CdSe shows a type-I band structure, when the materials were brought into direct contact, the band edges reorganize due to Fermi level alignment and forms a type-II band structure. [8-10]Apart from this, the consecutive CdS/CdSe passivation layers over Mn doped PbS can also favor more stability against the polysulfide electrolyte.

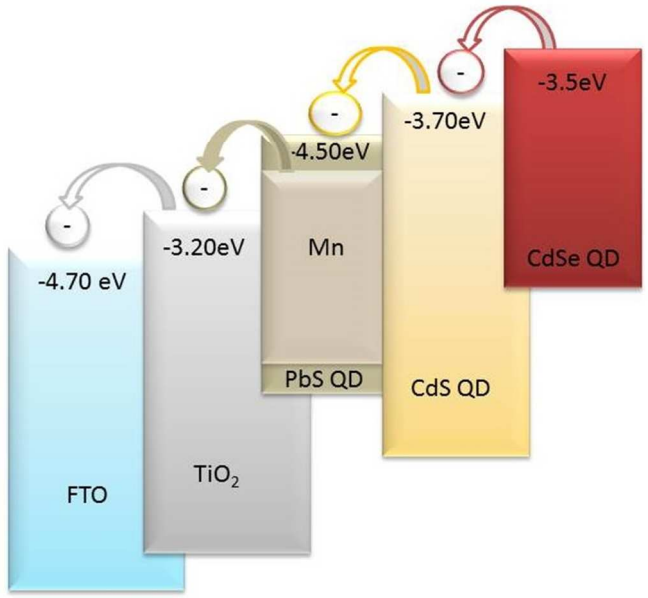

Fig. S2 Schematic representation of the energy band gap alignment of Mn-doped PbS/CdS/CdSe/ZnS sensitised TiO_2 films

1. Afriyanti Sumboja, Ce Yao Foo, Jian Yan, Chaoyi Yan, Raju Kumar Gupta and Pooi See Lee, Journal of material chemistry, 2012, **22**, 23921.
2. C. N. Borca, Delia Ristoiu. Q. L. Xu, S.-H. Liou, S. Adenwalla, and P. A. Dowbena, *Journal of applied physics*, 2000, **87**, 6104.
3. J. Deng, M. Wang, X. Song, Y. Shi, X. Zhang, J. *Colloid interface science*, 2012, **388**, 118-122.
4. J. Jiao, Z.J. Zhou, W.H. Zhou, S.X. Wu, *Material science in semiconductor processing*, 2013, **16**, 435-440.
5. A. Braga, S. Gimenez, I. Concina, A. Vomiero, I.M. Sero, *Journal of physical chemistry letters*, 2011, **2**, 454-460.
6. H. Lee, H.C. Leventis, S.J. Moon, P. Chen, S. Ito, S.A. Haque, T. Torres, F. Neuesch,T. Geiger, S.M. Zakeeruddin, M. Gratzel, M. Nazeerruddin, *Advanced functional materials*,2009,**19**, 2735-2742
7. I. Robel, M. Kuno, P.V. Kamat, *Journal of American Chemical society*, 2007, **129**, 4136-4137.
8. J.H. Bang, P.V. Kamat, *ACS Nano*, 2011, **5**, 9421-9427.
9. Y.L. Lee, C.F. Chi, S.Y. Liau, *Chemistry of materials*, 2010, **22**,922-927.
10. M. Seol, H. Kim, W. Kim, Y. Yong, *Electrochemistry communications*, 2010, **12,** 1416-1418.

]. See DOI: 10.1039/b000000x/

1. R.S. Selinsky, Q. Ding, M.S. Faber, J.C. Wright, S. Jin, *Chemical Society Reviews*, 2012, **42**, 2963-2985
2. P.V. Kamat, *Accounts of chemical research*, 2012, **45**, 1906- 1915.
3. J.H. Bang, P.V. Kamat, *ACS Nano,* 2009, **3**, 1467-1476.
4. X. Yu, B. Lei, D. Kuang, C. Su, *Journal of Materials Chemistry*, 2012, **22**, 12058-12063.
5. K.G.U. Wijayantha, L.M. Peter, L.C. Otley, *Solar Energy Materials and Solar Cells,* 2003 **83**, 363-369.
6. N. Fuke, L.B. Hoch, A.Y. Koposov, V.W. Manner, D.J. Werder, A. Fukui, N. Koide, H. Katayama, M. Sykora, *ACS Nano*, 2010, **4** , 6377-6386.
7. K.S. Leschkies, R. Divakar, J. Basu, E.E. Pommer, J.E. Boercker, C.B. Carter, U.R. Kortshagen, D.J. Norris, E.S. Aydil, *Nano Letters*, 2007, **7**, 1793-1798.
8. N. Balis, V. Dracopoulos, K. Bourikas, P. Lianos, *Electrochimica Acta,* 2013, **91**,246-252.
9. Q. shen, J kobayashi, Lina J, T.Toyoda, *Journal of Applied Physics,* 2012, **103**, 084304.
10. P.K. Santra, P.V. Kamat, *Journal of the American Chemical Society,* 2012, **134**, 2508-2511.
11. Y.-L. Lee, Y.-S. Lo, *Advanced Functional Materials,* 2009, **19**, 604-609.
12. N. Guijarro, J.M. Campina, Q. Shen, T. Toyoda, T. Lana-Villarreal, R. Gomez, *Physical Chemistry Chemical Physics, 2011*, **13,** 12024-12032.
13. C. Pejoux, S. Rühle, D. Cahen, G. Hodes, *Journal of Photochemistry and Photobiology A: Chemistry,* 2006, **181**, 306-313.
14. M. Nikumbh, V. Gore, R. B. Gore*, Renewable Energy*, 1997, **11**, 459-467.
15. A. Braga, S. Gimenez, I. Concina, A. Vomiero, I.M. Sero*, Journal of physical chemistry letters* ,2011, **2**, 454-460
16. J.B. Sambur, T. Novet, B.A. Parkinson, *Science,* 2010, **330**, 63-66.
17. B.R. Hyun, Y.W. Zhong, A.C. Bartnik, L. Sun, H.D. Abrun, F.W. Wise,J.D. Goodreau, J.R. Matthews, T.M. Leslie, N.F. Borrelli, *ACS Nano*, 2008, **2**, 2206-2212.
18. H. Lee, H.C. Leventis, S.J. Moon, P. Chen, S. Ito, S.A. Haque, T. Torres, F. Neuesch,T. Geiger, S.M. Zakeeruddin, M. Gratzel, M. Nazeerruddin, *Advanced Functional Materials,* 2009*,* **19**, 2735-2742.
19. C. Justin Raj a,*, S.N. Karthick b,c, Songyi Park b, K.V. Hemalatha b,d, Soo-Kyoung Kim b, K. Prabakar b, Hee-Je Kim, *Journal of Power Sources,* 2014 , **248**, 439-446.
20. Chia-Hao M. Chuang1, Patrick R. Brown, Vladimir Bulović and Moungi G. Bawendi , *nature materials*, 2014, **13** , 796-801
21. S. Buhbut, S. Itzhakov, D. Oron, A. Zaban, *Journal of physical chemistry letters*, 2011, **2**, 1917−1924.
22. H.Y. Fu, S.W. Tsang, Y.G. Zhang, J.Y. Ouyang, J.P. Lu, K. Yu, Y. Tao, *Chemistry of materials,* 2011, **23**, 1805-1810.
23. V. Chikan, *Journal of physical chemistry letters,* 2011, **2**, 2783−2789.
24. Chandu V. V. M. Gopi,[a] M. Venkata-Haritha, Soo-Kyoung Kim and Hee-Je Kim : DOI: 10.1039/c4dt03063j
25. Lyudmila Turyanska , Fabrizio Moro , Andrew N. Knott , Michael W. Fay , Tracey D. Bradshaw , and Amalia Patanè , *Particle & Particle Systems Characterization*, 2013, **30,** 945–949
26. G Long, B Barman, S Delikanli1, Y Tsung Tsai1, P Zhang, A Petrou1 and H Zeng , *Applied physics letters,* 2012, **101**, 062410 1-4
27. Haining Chen, Weiping Li, Huicong Liu, Liqun Zhu, *Microporous and Mesoporous Materials,* 2011,**138**, 235–238.
28. Haining Chen, Liqun Zhu, Huicong Liu, Weiping Li, *The Journal of physical chemistry C* ,2013, **117,** 3739−3746
29. S. Srinivasa Rao, Chandu. V.V.M. Gopi, Soo-Kyoung Kim, Min-Kyu Son, Myeong-Soo Jeong, A.Dennyson Savariraj, K. Prabakar, Hee-Je Kim, *Electrochimica Acta* , 2014 ,**133,** 174–179.
30. I Lim , D Yoon Lee, S. A. Patil , N. K. Shrestha a, S Hyung Kang ,Yoon-Chae Nah , W Lee ,Sung-Hwan Han, *Materials Chemistry and Physics* 2014, **148** , 562-568
31. L.H. Lai, L. Protesescu, M V. Kovalenko ,M. A. Loi, *Physical chemistry chemistry physics,* 2014, **16**, 736-74
32. K.M. Lee, V. Suryanarayanan, K.C. Ho, *Solar energy materials and solar cells* , 2007, **91**, 1416-1420.
33. Y.L. Lee, Y.S. Lo, *Advanced functional materials*, 2009, **19,** 604-609.
34. Q. Shen, J. Kobayashi, L.J. Diguna, T. Toyoda, *Journal of applied physics*, 2008, **103**, 084304-084305.
35. W.Q. Wu, B.X. Lei, H.S. Rao, Y.F. Xu, Y.F. Wang, C.Y. Su, D.B. Kuang, *Scientific reports* , 2013, **3**, 1352-1357.

36. J. Kim, H. Choi, C. Nahm, C. Kim, S. Nam, S. Kang, D.R. Jung, J.I. Kim, J. Kang, B.Park, *Journal of power sources,* 2012, **220**, 108-113.
37. T.L. Li, Y.L. Lee, H. Teng, *Energy and environmental science*, 2012, **5**, 5315-5324.
38. Haining Chen, Liqun Zhu, Huicong Liu, Weiping Li**,** *Electrochimica Acta,*2013,**105**, 289-298.
39. Qing Wang, Seigo Ito, Michael Gra1tzel,Francisco Fabregat-Santiago,Ivan Mora-Sero, Juan Bisquert, Takeru Bessho, and Hachiro Ima, *Journal of Physical Chemistry B***,** 2006,**110**, 25210-25221.
40. Haining Chen, Liqun Zhu, Huicong Liu, Weiping Li, *Journal of Power Sources,* 2014, **245**,406-410
41. Hee-Je Kim, Su-Weon Kim, Chandu V.V.M. Gopi, Soo-Kyoung Kim, S. Srinivasa Rao, Myeong-Soo Jeong, *Journal of Power Sources,* 2014, **268**, 163-170.
42. Hee-Je Kim, Tae-Bin Yeo, Soo-Kyoung Kim, S. Srinivasa Rao, A. Dennyson Savariraj, K. Prabakar and Chandu V. V. M. Gopi1, *European journal of inorganic chemistry,* 2014, 4281–4286.
43. Chandu V.V.M. Gopi, S. Srinivasa Rao, Soo-Kyoung Kim, Dinah Punnoose, Hee-Je Kim, *Journal of Power Sources* 2015, **275**,547-556
44. S. Srinivasa Rao, Chandu. V.V.M. Gopi, Soo-Kyoung Kim, Min-Kyu Son, Myeong-Soo Jeong, A. Dennyson Savariraj, K. Prabakar , Hee-Je Kim, *Electrochimica Acta,*2014 **133**,174–179

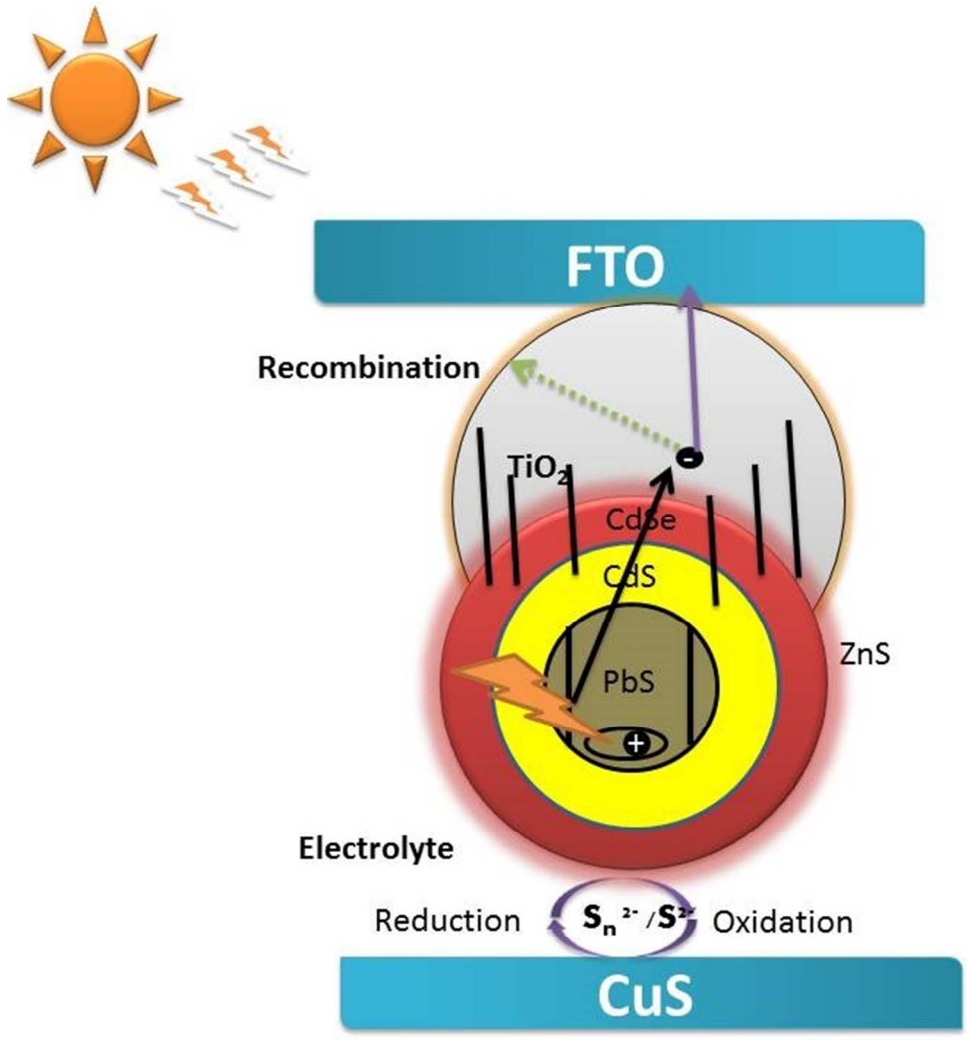

Better stability and higher performance of Mn-doped PbS/CdS/CdSe/ZnS QDSSCs (PCE=4.25%) than that of PbS/CdS/CdSe/ZnS (PCE=3.86%
180x189mm (96 x 96 DPI)